optica

Equivalent of the point spread function for partially coherent imaging

Shalin B. Mehta[1,*] and Colin J. R. Sheppard[2]

[1]Eugene Bell Center for Regenerative Biology & Tissue Engineering, Marine Biological Laboratory, Woods Hole, Massachusetts 02543, USA
[2]Nanophysics, Istituto Italiano di Tecnologia, via Morego 30, 16163 Genova, Italy
*Corresponding author: mshalin@mbl.edu

Received 21 May 2015; revised 28 June 2015; accepted 28 June 2015 (Doc. ID 240648); published 12 August 2015

Angularly diverse or partially coherent illumination is widely used for optical, x-ray, and electron microscopy. A long-standing challenge in developing new partially coherent approaches is that the nonlinear image formation model does not allow physical intuition into how the imaging and illumination pupils impact contrast and resolution. We report a phase-space model, the *phase-space imaging kernel*, for partially coherent systems that describes image formation in terms of a convolution and is analogous to the point spread function model for coherent imaging. We simulate phase-space imaging kernels for brightfield and differential interference contrast (DIC) microscopes to explain a seemingly paradoxical experimental result that the DIC image of a point depends on the coherence of the illumination. We discuss interpretation of the spatial and spatial-frequency marginals of the kernel. We expect this intuitive model and simulations to facilitate design of novel computational schemes for phase imaging and optical lithography.

OCIS codes: (050.5082) Phase space in wave optics; (110.4980) Partial coherence in imaging; (110.4850) Optical transfer functions; (220.3740) Lithography; (340.7440) X-ray imaging.

http://dx.doi.org/10.1364/OPTICA.2.000736

We have recently shown that imaging properties of a general partially coherent imaging system are elegantly represented by a particular phase-space distribution of the Cohen class, which we have termed the phase-space imager (PSI) [1]. We have shown that the PSI model can be used to compute images in different partially coherent microscope systems [2]. The PSI model represents the partially coherent system (consisting of the illumination and imaging pupils) in terms of a PSI-window that filters the specimen mutual spectrum. The PSI-window provides an efficient method of image computation, together with a direct link with Hopkins' transmission cross-coefficient (TCC) model [3], widely used in the optical lithography field. In this Letter, we develop an alternative description of the PSI that leads to deeper physical insight. This new description of partially coherent imaging is in terms of a system-dependent "kernel" that is convolved along the space dimension with the Wigner distribution of the specimen. The resulting description of the imaging process is the partially coherent generalization of the Wigner representation of coherent image formation.

We consider imaging of a thin (2D) specimen. The coherence of the imaging system is quantified by the coherence ratio $S = \mathrm{NA}_i/\mathrm{NA}$, where NA_i is the numerical aperture of illumination and NA is the numerical aperture of the imaging lens. Image formation due to a partially coherent system is bilinear in nature, i.e., the image intensity at a point in the image space depends on pairs of points of the specimen. For brevity, we describe coordinates in 2D space and spatial frequency as vectors indicated by boldface characters. We describe pairs of points $(\mathbf{x}_1, \mathbf{x}_2)$ by the center and difference coordinates $(\mathbf{x}, \mathbf{x}')$ in the normalized units of λ/NA, and pairs of spatial frequencies $(\mathbf{m}_1, \mathbf{m}_2)$ by the center and difference coordinates $(\mathbf{m}, \mathbf{m}')$ in the normalized units of NA/λ, where λ is the illumination wavelength. Therefore,

$$\mathbf{m} = \frac{1}{2}(\mathbf{m}_1 + \mathbf{m}_2), \qquad \mathbf{m}' = \mathbf{m}_1 - \mathbf{m}_2;$$
$$\mathbf{x} = \frac{1}{2}(\mathbf{x}_1 + \mathbf{x}_2), \qquad \mathbf{x}' = \mathbf{x}_1 - \mathbf{x}_2. \tag{1}$$

The expression for the PSI, as given as Eq. (5) in [1], is

$$\Psi(\mathbf{m}, \mathbf{x}) = \int T\left(\mathbf{m} + \frac{\mathbf{m}'}{2}\right) T^*\left(\mathbf{m} - \frac{\mathbf{m}'}{2}\right) C(\mathbf{m}, \mathbf{m}') \times \exp(2\pi i \mathbf{m}' \cdot \mathbf{x}) \mathrm{d}\mathbf{m}', \tag{2}$$

where $T(\mathbf{m})$ is the specimen spectrum and $C(\mathbf{m}, \mathbf{m}')$ is the PSI-window, basically a rotated version of the TCC of Hopkins' theory [3]. This implies that the PSI is represented as an inverse Fourier transform (along the $\mathbf{m}'$ dimension) of the specimen mutual spectrum $M(\mathbf{m}, \mathbf{m}') = T(\mathbf{m} + \mathbf{m}'/2)\, T^*(\mathbf{m} - \mathbf{m}'/2)$ filtered by the PSI-window. The model for the PSI, $\Psi(\mathbf{m}, \mathbf{x})$, can be summarized as

$$\Psi(\mathbf{m}, \mathbf{x}) = \mathcal{F}^{-1}_{m'}[M(\mathbf{m}, \mathbf{m}') C(\mathbf{m}, \mathbf{m}')]. \tag{3}$$

After transforming the quantities on the right-hand side according to the inverse Fourier transformation along $\mathbf{m}'$, we have

$$\Psi(\mathbf{m}, \mathbf{x}) = W(\mathbf{m}, \mathbf{x}) \otimes_{\mathbf{x}} K(\mathbf{m}, \mathbf{x}), \tag{4}$$

where $W(\mathbf{m},\mathbf{x}) = \mathcal{F}^{-1}_{m'}[M(\mathbf{m},\mathbf{m}')]$ is the Wigner distribution of the specimen's transmission, $K(\mathbf{m},\mathbf{x}) = \mathcal{F}^{-1}_{m'}[C(\mathbf{m},\mathbf{m}')]$ is the "kernel" we name the phase-space imaging kernel (PSI-kernel), and $\otimes_{\mathbf{x}}$ is the convolution of these two quantities along the spatial dimensions. Then, the image intensity is given by the spatial marginal of $\Psi(\mathbf{m},\mathbf{x})$ [1].

Note that the PSI is *not* the Wigner function associated with the image mutual intensity, and actually is not a Wigner function at all. It is a phase-space representation of the Cohen class in which the specimen and the imaging system can be separated (as in the TCC model), because the quantity of interest is image intensity and not mutual intensity. An analogous observation about separability has been made in the context of the matrix formulation of image formation [4]. The Wigner distribution of the image amplitude in a coherent imaging system (given by the convolution equation $i(\mathbf{x}) = t(\mathbf{x}) \otimes_{\mathbf{x}} h(\mathbf{x})$) is given by

$$W_i(\mathbf{m},\mathbf{x}) = W(\mathbf{m},\mathbf{x}) \otimes_{\mathbf{x}} W_h(\mathbf{m},\mathbf{x}), \tag{5}$$

where W_h is the Wigner distribution of the amplitude PSF, $h(\mathbf{x})$.

Equations (4) and (5) describe partially coherent and coherent imaging, respectively, both as linear operations between bilinear quantities. Models of partially coherent imaging in two dimensions involve four-dimensional quantities, and the PSI-kernel is an intuitive four-dimensional quantity that reduces to Wigner distribution of the PSF in the coherent limit. Therefore, the PSI-kernel provides a phase-space equivalent of the point spread function for partially coherent imaging.

Visualization 1 related to Fig. 1 shows the PSI-kernel of the brightfield microscope as the coherence of illumination is reduced by increasing the NA of the illumination. The kernel is displayed using a nested coordinate system, the outer coordinates describing the space coordinate and the inner coordinates describing the spatial frequency.

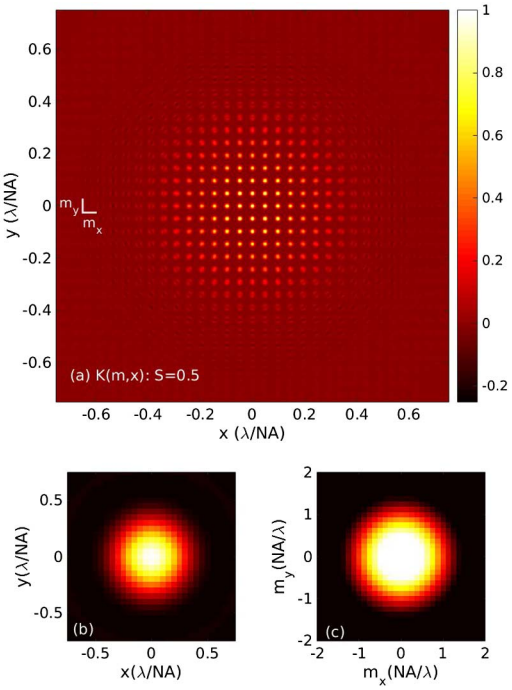

Fig. 1. Frame at $S = 0.5$ from Visualization 1. (a) The PSI-kernel of a brightfield microscope. The kernel is displayed using a nested coordinate system, the outer coordinates describing the space coordinates and the inner coordinates describing the spatial frequency. (b) The spatial marginal is the sum within inner tiles. (c) The frequency marginal is the sum of inner tiles.

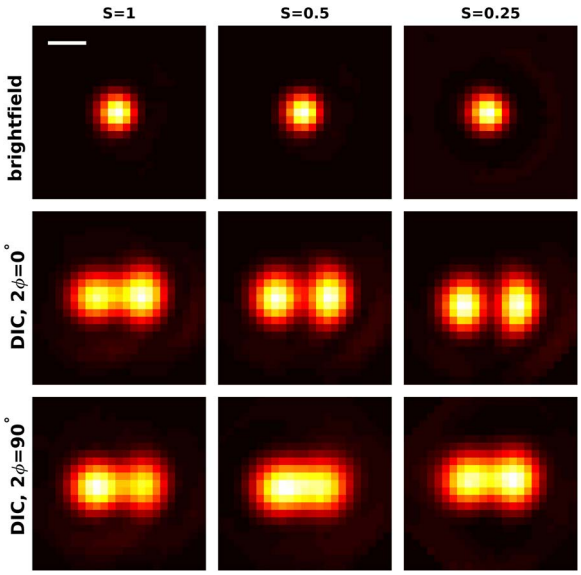

Fig. 2. Experimental images of a point under brightfield and DIC microscopes with multiple illumination aperture sizes. These are images of a point defect in an aluminum coating on a coverslip, acquired with 100× 1.3 NA objective at a wavelength of $\lambda = 532$ nm. The shear of the DIC prism was measured [5] to be $2\Delta = 0.5\lambda/\mathrm{NA}$, and bias ($2\phi$) was set to either 0° or 90°(180° bias provides brightfield-like contrast). Scale: 200 nm.

The spatial marginal of the PSI-kernel (the sum within inner tiles) is the image of a point and does not change with coherence of illumination, because a point is coherent with itself. Figure 2 shows experimental images of a point object in a brightfield microscope, and a DIC microscope at two different biases, each with varying NA of the illumination. It can be seen that the brightfield image of a finite-sized point changes negligibly with coherence of the illumination. It is well known that in a brightfield imaging system, the image of a point object is not affected by the illumination aperture, but is given simply by the point spread function.

The frequency marginal (the sum of the inner tiles) of the PSI-kernel changes with coherence of illumination. It is the same as the modulation transfer function (MTF) for coherent illumination and the phase-gradient transfer function (PGTF) for partially coherent illumination, as discussed later. Note that the PSI-kernel is real valued, but can be negative valued to account for interference effects, e.g., in microscopes with significant coherence and in the differential interference contrast (DIC) microscope.

In what seems to be paradoxical behavior, the DIC image of the point in Fig. 2 is affected by the coherence of the illumination. Moreover, the change in the image due to coherence is the least pronounced with bias of 90° and the most pronounced with bias of 0°. These results can be simulated with purely spatial representation of partially coherent imaging [6], but that does not clarify the physical reason for the observation. Computing and observing the PSI-kernel of the DIC microscope and its marginals can explain this apparent paradox.

Assuming that the direction of shear in a DIC microscope is along the x axis, the expression for the PSI-window of

the DIC microscope (from Eq. (15) of [7] and Eq. (10) of [2]) is

$$C_{\mathrm{DIC}}(\mathbf{m},\mathbf{m}') = C(\mathbf{m},\mathbf{m}')\sin\left[2\pi\left(m_x - \frac{m_x'}{2}\right)\Delta - \phi\right] \times \sin\left[2\pi\left(m_x + \frac{m_x'}{2}\right)\Delta - \phi\right] = C(\mathbf{m},\mathbf{m}')[\cos(2\pi m_x'\Delta) - \cos(4\pi m_x\Delta - 2\phi)], \quad (6)$$

where $C(\mathbf{m},\mathbf{m}')$ is the PSI-window of a brightfield microscope, (m_x, m_x') are frequency coordinates along the direction of shear, 2Δ is the shear, and 2ϕ is the bias. The PSI-kernel of the DIC microscope then is the inverse Fourier transform of $C_{\mathrm{DIC}}(\mathbf{m},\mathbf{m}')$ along the $\mathbf{m}'$ dimension:

$$K_{\mathrm{DIC}}(\mathbf{m},\mathbf{x}) = K(\mathbf{m},\mathbf{x}) \otimes_{\mathbf{x}} [\delta(x-\Delta) + \delta(x+\Delta) - \delta(x)\cos(4\pi m_x\Delta - 2\phi)]. \quad (7)$$

The expression in the square brackets is recognizable as the Wigner distribution of two points separated by 2Δ with mutual phase of 2ϕ. Thus, the PSI-kernel of the DIC microscope is given as the convolution of the PSI-kernel of the brightfield microscope and the Wigner distribution of two points separated by the shear of the microscope. This is expected, because the DIC microscope interferes coherently the light produced by two shifted copies of the specimen, as seen from Eq. (7) in [7]. Since the DIC microscope effectively images two points separated by the shear distance when the specimen is single-point, the image depends on the coherence of illumination.

Visualization 2 related to Fig. 3 displays the simulated PSI-kernel of the DIC microscope for zero bias at varying coherence,

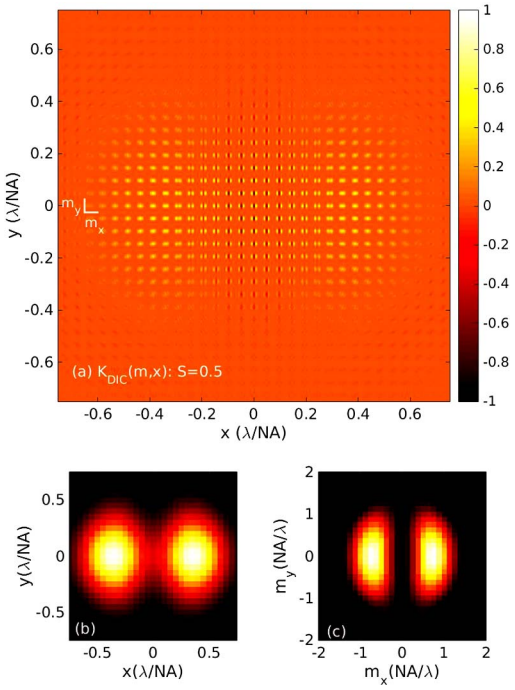

Fig. 3. Frame at $S = 0.5$ from Visualization 2. (a) The simulated PSI-kernel of the DIC microscope with shear of $0.5\lambda/\mathrm{NA}$ and bias of 0°, (b) the spatial marginal of the PSI-kernel, or the DIC image of a point, and (c) the frequency marginal of the PSI-kernel.

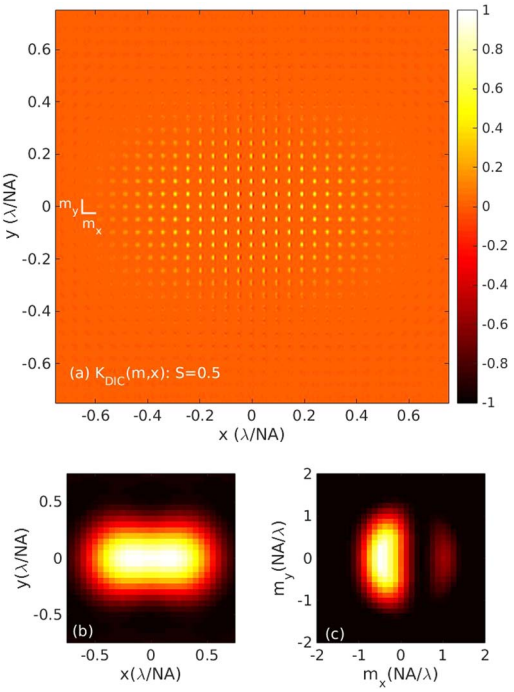

Fig. 4. Frame at $S = 0.5$ from Visualization 3. (a) The simulated PSI-kernel of the DIC microscope with shear of $0.5\lambda/\mathrm{NA}$ and bias of 90°, (b) the spatial marginal of the PSI-kernel, or the DIC image of a point, and (c) the frequency marginal of the PSI-kernel.

which illustrates the effect on the PSI-kernel of the brightfield microscope of convolution with the Wigner distribution of the two points. The DIC image of a point is shown as a spatial marginal of the kernel, and matches well with the experimental images acquired with zero bias in Fig. 2. Figure 4 (Visualization 3) shows simulation similar to Fig. 3, but with bias of 90°. Remarkably, the simulated DIC image of a point in Visualization 3 appears unaffected by the coherence of illumination. This simulated image matches well with experimental images in Fig. 2, bottom row—the slight mismatch is due to experimental error in setting the bias of 90° precisely. Thus, simulating the PSI-kernel and its spatial marginal clarifies the apparently paradoxical observations made with the DIC microscope. Figures 1, 3, and 4 also show the frequency marginal of PSI-kernel, whose interpretation is discussed next.

Since the spatial marginal and the spatial-frequency marginal of the Wigner distribution of the image amplitude [W_i in Eq. (5)] are the image intensity and the power spectrum of the image, respectively, it is natural to ask what the marginals of the PSI and the PSI-kernel imply. We have already shown that the spatial marginal of the PSI is the image intensity produced by a partially coherent system [1].

The frequency marginal of the PSI, from Eq. (3), is

$$\int \Psi(\mathbf{m},\mathbf{x})\mathrm{d}\mathbf{x} = \int \mathcal{F}^{-1}_{m'}[M(\mathbf{m},\mathbf{m}')C(\mathbf{m},\mathbf{m}')]\mathrm{d}\mathbf{x}. \quad (8)$$

Recognizing that the $\mathbf{m}'$ and $\mathbf{x}$ are Fourier conjugate variables, and therefore projection along $\mathbf{x}$ implies taking a slice in the Fourier domain along $\mathbf{m}' = \mathbf{0}$, the frequency marginal of the PSI can be written as

$$\int \Psi(\mathbf{m},\mathbf{x})\mathrm{d}\mathbf{x} = M(\mathbf{m},\mathbf{0})C(\mathbf{m},\mathbf{0}), \quad (9)$$

where $M(\mathbf{m}, \mathbf{0}) = |T(\mathbf{m})|^2$ is the power spectrum of the specimen transmission. Substituting $\mathbf{m}' = \mathbf{0}$ in Eq. (6) of [1] shows that $C(\mathbf{m}, \mathbf{0}) = |P(\mathbf{m})|^2 \otimes |P_i(\mathbf{m})|^2$ is the convolution of the magnitudes of the imaging pupil P and illumination pupil P_i.

The coordinate $\mathbf{m}$ of Wigner distribution is the instantaneous spatial frequency, which is defined as the derivative of the local phase for analytic signals [8]. Therefore, $C(\mathbf{m}, \mathbf{0})$, the frequency marginal of the PSI-kernel, describes how instantaneous frequencies of the specimen contribute to the image. In fact, it is identical to the phase gradient transfer function (PGTF) for slowly varying specimens [9,10], which gives the image intensity for a constant phase gradient object. The asymmetric form of the frequency marginal (PGTF) for DIC in Fig. 4(c) has been noted previously, and is responsible for highlighting and shadowing in DIC images [11].

For coherent illumination, i.e., $P_i(\mathbf{m}) = \delta(\mathbf{m})$, the quantity $C(\mathbf{m}, \mathbf{0}) = |P(\mathbf{m})|^2$ is the modulation transfer function (MTF) of the coherent system, i.e., the squared modulus of the coherent transfer function. For coherent systems, the product of the power spectrum of the specimen and the MTF is the power spectrum of the image amplitude.

For partially coherent systems the image amplitude is not defined, and the signal with real spatial frequency $\mathbf{f}$, i.e., $\cos(2\pi\mathbf{f} \cdot \mathbf{x})$, is not localized in the Wigner domain. Slowly varying objects and certain analytic signals have localized Wigner distributions and their images can be intuitively interpreted in terms of the frequency marginal of the PSI-kernel. Consider an analytic signal of the form

$$t(\mathbf{x}) = a(\mathbf{x}) \exp[i2\pi\mathbf{m}_0(\mathbf{x}) \cdot \mathbf{x}]. \tag{10}$$

Here, for a single analytic spatial frequency, $a = 1$, $\mathbf{m}_0(\mathbf{x}) = \mathbf{f}$, and for a linear chirp signal, $a = 1$, $\mathbf{m}_0(\mathbf{x}) = f\mathbf{x}$. For the general case of a slowly varying specimen, the modulus a and the instantaneous frequency $\mathbf{m}_0$ can be regarded as locally constant such that $2\pi\mathbf{m}_0$ represents the local phase gradient. The Wigner distribution function of such a specimen,

$$W(\mathbf{m}, \mathbf{x}) = a^2(\mathbf{x})\delta[\mathbf{m} - \mathbf{m}_o(\mathbf{x})], \tag{11}$$

is a delta line in phase space. Convolution with this delta line samples the PSI-kernel along the trajectory of the line. Then there is only a single instantaneous spatial frequency present at any position $\mathbf{x}$, so that $\mathbf{m}' = \mathbf{0}$ and the image intensity is simply

$$I(x) = a^2(\mathbf{x})C[\mathbf{m}_o(\mathbf{x}), \mathbf{0}]. \tag{12}$$

For a linear chirp object, Eqs. (11) and (12) are exact, whereas for a general variation of phase, the phase must be slowly varying for the Wigner distribution function to be approximated by a delta-line in phase space.

In summary, we have shown that imaging in a partially coherent imaging system such as an optical, x-ray, or electron microscope can be modeled as a filtering of the Wigner distribution function of the object. Specifically, the filtering corresponds to taking the spatial marginal of the space convolution with a system-dependent phase-space kernel, called the PSI-kernel. The method can be applied to brightfield or phase contrast systems. In the limit of a slowly varying object, as will be the case if the Rytov approximation is valid, the model much simplifies to give a spatially varying intensity that depends on the local phase gradient of the sample according to the frequency marginal of the PSI-kernel.

Funding. Human Frontier Science Program (HFSP) (LT000096/2011-C).

REFERENCES

1. S. B. Mehta and C. J. R. Sheppard, Opt. Lett. **35**, 348 (2010).
2. S. B. Mehta and C. J. R. Sheppard, J. Mod. Opt. **57**, 718 (2010).
3. H. H. Hopkins, Proc. R. Soc. London **217**, 408 (1953).
4. K. Yamazoe, J. Opt. Soc. Am. A **29**, 2591 (2012).
5. S. B. Mehta and C. J. R. Sheppard, Appl. Opt. **49**, 2954 (2010).
6. S. B. Mehta and R. Oldenbourg, Biomed. Opt. Express **5**, 1822 (2014).
7. S. B. Mehta and C. J. R. Sheppard, Opt. Express **16**, 19462 (2008).
8. J. Ville, Cables et Transmissions **2A**, 61 (1948) [translated from French in 1958 by I. Selin of the RAND Corporation].
9. C. J. R. Sheppard, D. K. Hamilton, and I. J. Cox, Proc. R. Soc. Lond. A **387**, 171 (1983).
10. D. K. Hamilton and C. J. R. Sheppard, J. Microsc. **133**, 27 (1983).
11. C. J. Cogswell and C. J. R. Sheppard, J. Microsc. **165**, 81 (1992).